Robust Maneuverability of a Miniature, Low-Cost Underwater Robot using Multiple Fin Actuation

Florian Berlinger, Jeff Dusek, Melvin Gauci, and Radhika Nagpal

***Abstract*—In this paper we present the design of a miniature (100 mm) autonomous underwater robot that is low-cost ($ 100), easy to manufacture, and highly maneuverable. A key aspect of the robot design that makes this possible is the use of low-cost magnet-in-coil actuators, which have a small profile and minimal sealing requirements. This allows us to create a robot with multiple flapping fin propulsors that independently control robot motions in surge, heave, and yaw. We present several results on the robot, including: (i) quantified open-loop swimming characteristics; (ii) autonomous behaviors using a pressure sensor and an IMU to achieve controlled swimming of prescribed trajectories; (iii) feedback from an optic sensor to enable homing to a light source. The robot is designed to form the basis for underwater swarm robotics testbeds, where low cost and ease of manufacture are critical, and 3D maneuverability allows testing complex coordination inspired by natural fish schools. Individually, miniature and low-cost underwater robots can also provide a platform for the study of 3D autonomy and marine vehicle dynamics in educational and resource-constrained settings.**

***Index Terms*—marine robotics, biologically-inspired robots, swarms**

I. Introduction

UNDERWATER robot collectives have the opportunity to expand the capabilities of marine exploration by creating mobile and distributed sensor networks, improving mission scalability and robustness, and reducing the risk of operation in cluttered and complex environments. Underwater operation presents unique challenges from a collective robotics perspective, beyond those encountered in ground-based systems. Severe limitations are placed on sensing and communication modalities; additionally, motion is in 3-dimensions (3D) with non-negligible inertial effects and hydrodynamic coupling between nearby robots. One approach to developing future marine swarms is to build a lab-based swarm testbed to gain algorithmic knowledge in a controlled still-water environment that can be transferred to sophisticated agents in higher-risk real-world settings. The confines of a laboratory environment place the design emphasis on small size and high maneuverability over straight-line speed. Additionally, the utilization of off-the-shelf components allows for scalability through low cost and ease of manufacture.

Laboratory-scale research in underwater robotics includes, on the one hand, miniature, low-cost robots (e.g., $\leq$ 100 mm, $ 100) with low maneuverability and/or low reliability, and on the other hand, highly-maneuverable and reliable robots that are large and expensive due to their complexity (e.g., $\geq$ 300 mm, $ 1000). The contribution of this paper is the design of an underwater robot that bridges this gap. The robot is 100 mm in the longest dimension and has a component cost of $ 100. Despite its minimal design, the robot achieves a high level of maneuverability in 3D, including on-the-spot turning and in-place depth variation. Furthermore, experiments in a controlled environment demonstrate the robot's ability to perform autonomous behaviors. These include repeatable ascent and descent using a pressure sensor, 3D trajectory following using a pressure sensor and an IMU, and robust homing towards an optical beacon using a photodiode.

II. Related Work

Several groups have designed miniature robots for lab environments. Most examples involve a single actuator system to achieve low cost and small size. Kopman et al. presented a robot (117 mm in length, $100) with a fin actuated by a waterproof servomotor [1], aimed at STEM education. In Clark et al.'s robot (58 mm) a fin is driven by a magnet-in-coil (MIC) actuator [2]. Yet other designs have driven fins by piezo-electric actuators, such as the one by Aureli et al. [3] (100 mm). In these single-fin robots, forward motion is achieved by symmetric flapping of the fin, and large-radius turning (i.e., not on-the-spot) is achieved by biasing the flapping. Takada et al. [4] presented a robot with a fin driven by a MIC actuator as in [2]; in addition to planar motion, this robot is also able to pitch using an internal servomotor that shifts the robots center of mass. All of these examples rely on flapping actuation, in part because propellers are hard to miniaturize while still sealing the moving mechanism in a way that is reliable. Toy submarines for example can be based on small propellers however their reliability is extremely limited.

At slightly larger sizes ($\sim$250 mm), several groups have designed 3D maneuverable robots using multiple actuators including propellers, servomotors, and pumps [5]. For example, the Jeff robot (250 mm, $1300) was designed as part of the CoCoRo project, and is intended for operation in collectives [6]. It uses two vertically-stacked propellers at the back for forward

Manuscript received: February 15, 2017; Revised May 7, 2017; Accepted July 10, 2017.

This paper was recommended for publication by Editor Jonathan Roberts upon evaluation of the Associate Editor and Reviewers' comments. This work was supported by the Wyss Institute for Biologically Inspired Engineering.

This letter has supplementary downloadable material available at http://ieeexplore.ieee.org including a video of robot capabilities and further analysis of the MIC propulsor

The authors are with the John A. Paulson School of Engineering and Applied Science at Harvard University, Cambridge, Massachusetts. E-mails: {fberlinger@seas, jdusek@g, mgauci@g, rad@eecs}.harvard.edu

Digital Object Identifier (DOI): see top of this page.

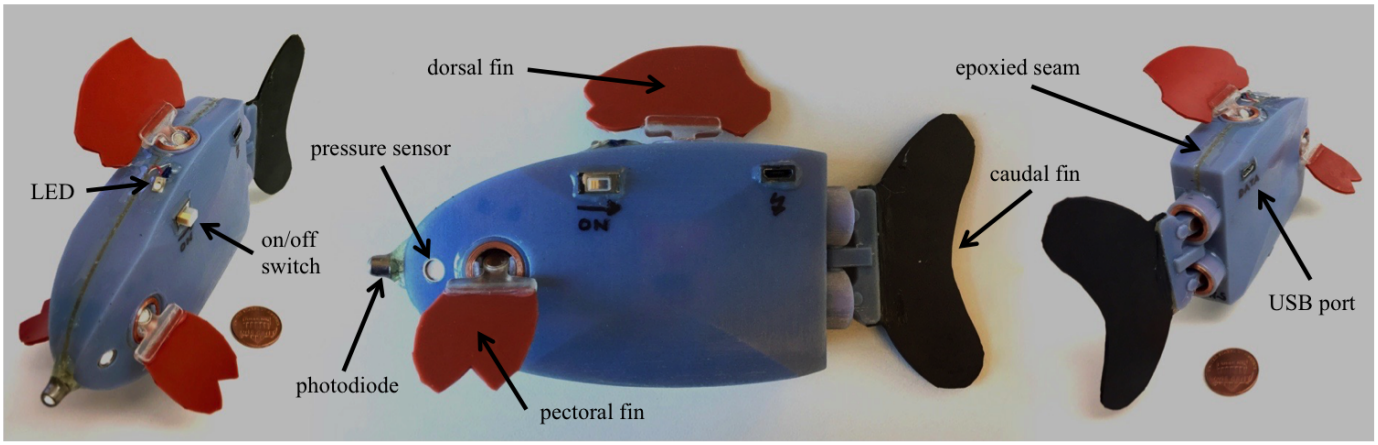

Fig. 1. The assembled robot, showing the four propulsors, the external sensors, and electronic components.

motion and pitch variation, another propeller for turning on the spot, and piston-based buoyancy modulation for in-place depth control. The propellers use custom-designed magnetic shaft couplings, which are relatively large and expensive but eliminate the waterproofing issues associated with a body-penetrating shaft. Other robots in this range use flapping-fin based designs, with both rear/caudal and side/pectoral fins controlled by multiple servomotors. Examples include the Jessiko robot [7] (220 mm) and the boxfish-inspired robot by Hu et al. [8] (350 mm). The use of multiple flapping fins allows these robots to achieve forward motion, turning, pitch control, and in some cases rapid braking. A third propulsion mechanism for 3D maneuverability is the use of multiple internal pumps. For example the robot by Bhattacharyya et al. [9] (203 mm) uses four internal pumps to suck water from inlets and distribute it to outlets, creating jets to control five degrees of freedom. The robots described in this paragraph, while having high degrees of maneuverability and reliability, use sophisticated means of actuation that are not easily scaled down in size and cost.

In our design, we develop a robot with multiple propulsors to control 3D motion using an actuation strategy that is easy to manufacture (no complex sealing hardware), low-cost, and small profile. To achieve this, we took inspiration from one of the actuators used in miniature robots, namely the magnet-in-coil (MIC) actuator [2], [4], and modified it for a multiple fin design. We show that this robot is capable of considerably more complex motion and autonomous control than previous miniature robots, as a result of the increased maneuverability.

III. Robot Design

Our design goal was to create a robot that is miniature, low-cost, easy to manufacture, reliable, and capable of 3D autonomous movement. Figure 1 shows the robot's exterior. The component cost is around $ 100, and the overall dimensions (excluding the fins) are: 100 mm in length; 60 mm at the highest point; 25 mm at the thickest point; and 125 g in mass. Multiple flapping fins used for locomotion make the robot capable of forward motion, vertical ascent and descent, and on-the-spot turning. Roll and pitch are stabilized passively by the robot's mechanical design.

Body Design: The robot's exterior consists of a plastic body, 3D printed in two halves on a Stratasys Objet500, and four fins made from flexible rubber. The shape of the body has elliptical profiles in height and thickness in order to reduce hydrodynamic form drag. Additionally, the body has a 'flat' profile along the plane defined by the surge and heave axes, which increases the added mass in sway and yaw. This helps reject oscillations induced on the body by the flapping fins, improving straight-line swimming efficiency.

Propulsor Design: Achieving a four-fin configuration within our design constraints is made possible by using *magnet-in-coil (MIC) propulsors* [2], [4], which offer the following advantages: (i) they are easy to miniaturize; (ii) they have no moving components that penetrate the body of the robot, which makes for easier waterproofing; (iii) they are low-cost, with a current cost of around $ 1/unit.

A single MIC propulsor is shown in Figure 2 in both the disassembled and assembled states. The assembly process starts by mounting a coil (a) inside a housing (b). A cylindrical magnet (c) is mounted inside a separate housing, which is part of a hinge that also contains a slit for a fin (d). The hinge is then mounted inside the coil housing, with two pins on the hinge sliding into two grooves on the coil housing. This lets the hinge rotate along one axis inside the coil housing, with a mechanically-constrained amplitude of $\pm 20^\circ$. Two plugs (e) are fixed inside the grooves to prevent the hinge from becoming detached, and from moving or rotating in all other axes. The assembly is completed by attaching a rubber fin to the slit on the hinge (f). The MIC propulsor works by passing a current through the coil with a periodically alternating direction. The magnet 'attempts' to align its own magnetic field with the magnetic field inside the coil, which imparts motion on the hinge. An H-bridge controlled from a microcontroller achieves the required alternating current with controllable frequency.

The MIC actuator parameters were chosen based on the desired robot dimensions, speed, and power constraints. In the supplementary information, we derive scaling laws for the actuator's torque efficiency. It turns out that the efficiency scales inversely linearly with the overall size, number of layers (in the radial direction), and current; and scales inversely

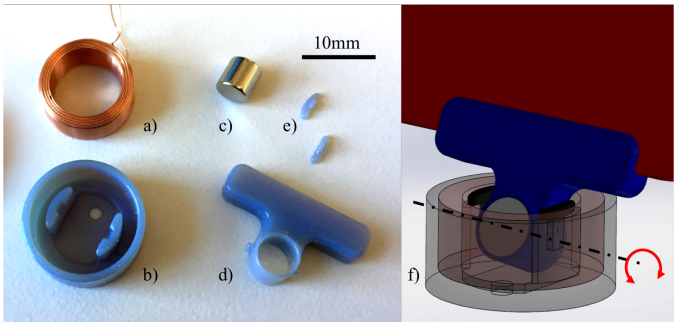

Fig. 2. Modular MIC propulsor: a) electromagnetic coil; b) propulsor housing with mounts for the coil and the hinge, and with a hole for the power cables; c) permanent magnet; d) flapping hinge with mounts for the magnet and the fin; e) plugs that hold the hinge in place; f) semi-transparent CAD of the assembled propulsor with an indicated rotary axis.

quadratically with the turns density (number of turns per unit length; equal to the reciprocal of the wire diameter). Therefore, the more torque that is desired, the less efficiently it will be generated, showing that the MIC actuator is only practical at small scales. As a of rule of thumb, one should achieve the desired torque by the following procedure. Begin by choosing the strongest appropriately-sized permanent magnet available. Set the inner coil diameter and the coil height to *just* accommodate the magnet; any extra space will result in unused magnetic field that increases power consumption but not torque. Achieve the desired torque by increasing the current, number of layers, and turns density, with a preference to increase them in that order.

Our desired robot thickness at the back is 16 mm. We chose a 5x5 mm cylindrical neodymium magnet with a high pull force of 16.9 N. Accordingly, the inner diameter and height of the coil were set to 9.2 mm and 5.5 mm. The coil consists of 200 turns of 0.18 mm thick copper wire (not accounting for insulation). This corresponds to 7 layers in the radial direction, an outer diameter of 12.3 mm, and a turns density of 5 turns/mm. The resistance of the coil is 5 Ω, which lets 1 A pass through at 5 V. This gives a reasonable runtime with the available energy density and was empirically found to yield an adequate acceleration and top speed of the robot.

Maneuverability: The caudal/rear fin is actuated by two MICs, and provides thrust in the surge (forward) direction when its flapping is symmetrical; by biasing its flapping, it can also be used to provide large-radius turning. The two pectoral/side fins, actuated by one MIC each, can be activated one at a time to make the robot turn in yaw; if the caudal fin is not activated during this time, the robot is able to turn almost on the spot. The dorsal/top fin, actuated by one MIC, allows for vertical diving in the heave direction. Vertical ascent is achieved implicitly by manufacturing the robot such that its weight makes it *slightly* positively buoyant in water (around 1 g under the neutrally-buoyant weight). As such, deactivating the dorsal fin makes the robot ascend slowly, and reactivating it stops the ascent almost immediately. The robot is designed to be passively straight and stable along the pitch and roll axes. This is achieved by distributing the mass internally such that the center of mass is significantly lower than and directly below the center of buoyancy. Passive stability and consistent orientation mitigate the coupling of heave with roll and yaw motions.

Computation and Sensors: The robot has an Arduino Pro Mini microcontroller and three sensors: (i) A 9-axis accelerometer (InvenSense MPU-9250) inside the body provides linear accelerations and rotational velocities in three dimensions. Although it also provides magnetic field readings, we do not use these due to interference from the MIC propulsors. (ii) A pressure sensor (TE Connectivity MS5803-02BA), mounted on the side of the robot, can provide pressure readings up to a depth of 10 m with a resolution of up to 0.25 mm. (iii) A blue light photodiode (Excelitas Technologies VTP1112H), mounted at the front of the robot with a viewing angle of $\pm 15^{\circ}$, measures light intensity. In addition to these sensors, an SD card reader/writer is included inside the robot for data logging, and a blue light LED is placed at the top for signalling. All the electronics, as well as the MIC propulsors, are powered from a single-cell (3.7 V, 320 mAh) Li-Ion battery. Data transfer and charging are accomplished via waterproof USB ports.

Manufacturability: We aimed to make the robot easy to manufacture and assemble reliably within approximately $8-10$ person-hours as follows. The body and MIC propulsor housings are 3D-printed, and any support material is removed with a waterjet cleaner. The MIC propulsors are assembled as described above, and are mounted on the robot's body. The circuitry is soldered together using 36-gauge ultra-flexible wire, and electronic components are mounted inside the body and fixed as necessary using foam mounting double-sided tape or liquid adhesive. Some internal weights are added in predetermined locations for approaching (with some leeway) the desired buoyancy, and pitch and roll straightness and stability. Next, the components that penetrate the hull are coated with plastic-bonding epoxy from the inside for waterproofing purposes. The robot is then closed by joining the two halves of the hull and applying plastic-bonding epoxy over the seam. The robot is placed in water and external trimming weights are added as necessary.

IV. Experimental Setup

Experiments were conducted in fresh water in a testing and visualization tank which measures 1.78 m x 1.78 m x 1.17 m (water depth 0.91 m). The tank is constructed from fiberglass with a white gelcoat interior and two 0.61 m x 0.91 m polycarbonate viewing windows. This allows for 3D tracking of the underwater robot using a pair of DSLR cameras mounted outside of the tank. The primary tracking camera was mounted from an overhead gantry above the tank and provided x-y localization in the fluid volume, as seen in Figure 3. The second camera was mounted on a tripod, looking into the fluid volume along the x-axis through one of the polycarbonate viewing windows. Using the two orthogonal camera views, the refraction in the images at the two air-water interfaces can be solved simultaneously, allowing for 3D localization of the robot in the tank reference frame based on [10].

The accuracy of the 3D tracking method was verified using fixed targets at known locations in the tank, and by comparing the robot depth from the visual tracking to the depth calculated

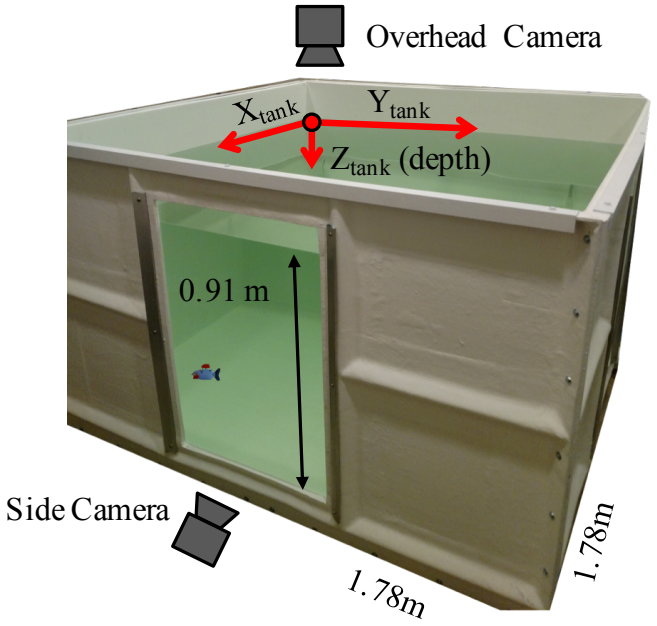

Fig. 3. 3D tracking of the robot's position in a fresh water testing tank was accomplished using two DSLR cameras oriented along the tank's X and Z axes respectively. Robot trajectories were referenced to a coordinate system fixed at the tank corner and with the Z coordinate (depth) measured down from the free surface.

from on-board pressure measurements, as shown in Figure 4. Localization accuracy was found to be within approximately 1/2 body length in the x-y plane, and 1/2 body height in depth. Errors in the visual tracking can be attributed to offsets between the robot centroid identified in image processing and the on-board sensors, as well as slight alignment errors between the two camera axes and the tank reference frame.

V. Results

Our robot design explained in Section III meets the goals of miniature size and low cost. In this Section, we demonstrate the 3D maneuverability and autonomous behavior capabilities of the robot. We present results on the robot's swimming performances in open-loop configurations and closed-loop autonomous behaviors with interoceptive (pressure sensor, IMU) and exteroceptive (photodiode) sensors. We also compare our robot's performance to previous robot designs.

All of the experiments were taken in a submerged state. Experimental data was obtained by logging readings from the robot to an on-board SD card, and by the external tracking system. A control loop updated the robot's behavior at 10Hz.

A. Open-loop Swimming Characteristics

Table I shows the robot's actively and independently controlled swimming characteristics for surge, heave, and yaw. In all cases, the robot's roll and pitch were passively stable thanks to its mass distribution, and sway was minimized thanks to its shape (see Section III). We use the normalized metrics of body lengths and body lengths per second, which allow for a fair comparison to similarly-sized robots (for our robot, 1 BL = 100 mm).

Metric	Value	Units	Propulsor
Forward Swim Speed	0.6	BL/s	Caudal at 2.2 Hz
Turn Radius from Rest	1.2	BL	Caudal biased
Turn Radius from Rest	0.5	BL	Pectoral at 1.0 Hz
Turn Radius Gliding	1.0	BL	Pectoral at 1.0 Hz
Descending Rate	0.17	BL/s	Dorsal at 2.8 Hz
Ascending Rate	0.26	BL/s	Passive

TABLE I
Open-loop Swimming Characteristics.

1) Forward Swimming Speed: The maximum forward swimming speed of our robot is 0.6 BL/s. The choice of a double actuator for powering the caudal fin was justified by comparing its speed and energy consumption against an identical fin powered by a single actuator. The double actuator consumed twice as much energy but resulted in three times the swimming speed. We consider the current swimming speed of our robot to be adequate for our purpose of testing in controlled, small-size environments. Furthermore, we expect that a moderate increase in normalized speed (i.e., in BL/s) will be achieved through refining fin and body shape, and miniaturizing the robot further.

2) Turning Radius: The robot's turning radius was evaluated in a number of different ways. (i) The robot started from rest, and turning was achieved by activating only the caudal fin in a biased manner (i.e., flapping from the center to one side). This turning radius was 1.2 BL. (ii) The robot started from rest, one pectoral fin was activated, and the caudal fin was fixed at one extreme to act as a rudder and support the turning. This turning radius was 0.5 BL. (iii) To characterize more typical operation, the caudal fin was first activated and the robot allowed to reach steady-state speed. The caudal fin was then deactivated (but again fixed at one extreme to act as a rudder), and one pectoral fin was activated while the robot was gliding. This turning radius was 1 BL. The comparison of (i) and (ii) justifies the addition of pectoral fins as they allow nearly on-the-spot turning. Furthermore, the pectoral fins decouple turning from forward swimming.

3) Descending and Ascending Rates: The robot descends vertically when the dorsal fin is activated, and ascends vertically due to its positive buoyancy when the dorsal fin is deactivated. The ascending and descending rates depend on the margin of positive buoyancy and on the thrust force available from the dorsal fin. We aimed at roughly equal rates for descending (0.17 BL/s) and ascending (0.26 BL/s). This is achieved by tuning the buoyancy such that the lift force equals half the thrust force available from the dorsal fin.

4) Comparison to Other Robots: The forward swimming speed of our robot (0.6 BL/s) is in the same range as similar flapping-based robots, such as Kopman et al. [1] (0.85 BL/s), Clark et al. [2] (0.63 BL/s), Aureli et al. [3] (0.08 BL/s), and Jessiko [7] (1 BL/s). Achieving significantly higher swimming speeds than these is definitely possible, but comes at the cost of either increased complexity or decreased reliability. For example, propellers can be driven from internal motors by sophisticated mechanisms such as magnetic couplings (see Figure 3 in [6]), or by greased body-penetrating shafts, which require regular maintenance. Interestingly, significantly higher speeds than the one achieved here (up to 11.6 BL/s) have also

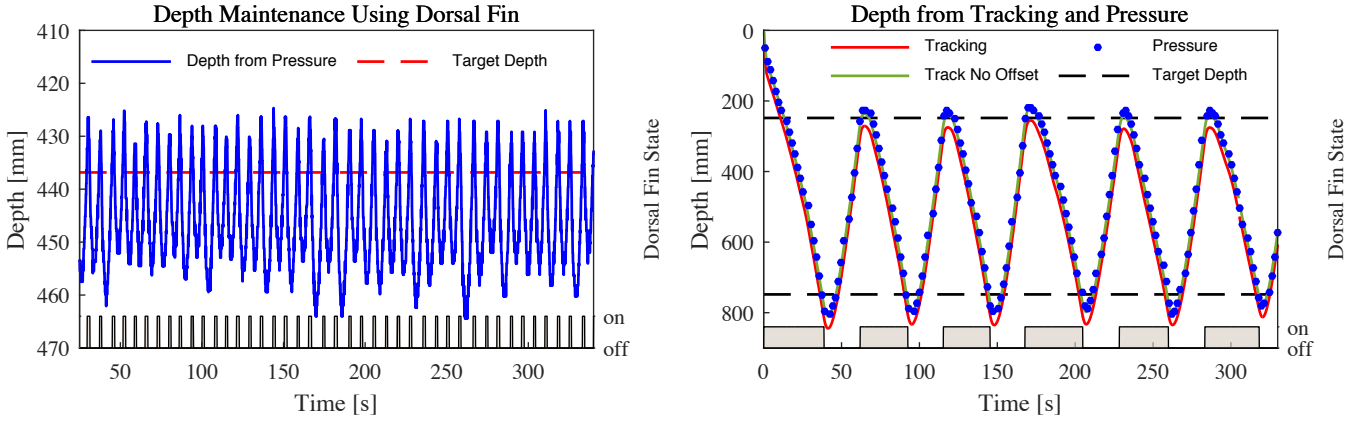

Fig. 4. **Left:** Active maintenance of target depth (red dashed line) using pressure sensor feedback and dorsal fin actuation to oppose positive buoyancy. **Right:** Test of diving performance between target depths of 248 mm and 748 mm. The red line denotes the robot depth from visual tracking, and the blue circles denote depth found from pressure sensor measurements (samples shown every 2 s for clarity). The green line denotes the depth from visual tracking with a constant offset of 30 mm (∼1/2 body height) removed.

been demonstrated with flapping-based motion, but at the cost of a highly-complex, multiple-joint body [11].

Two significant limitations in our robot's locomotion are the lack of ability to brake forward motion, and to move backwards. These capabilities are exhibited by robots such as Jeff [6], Jessico [7], and the 'boxfish' [8]. Initial experiments utilizing angled pectoral fins on the robot have demonstrated the ability to generate backward thrust when activated simultaneously, providing a pathway to filling this capability gap without added complexity.

The minimal turning radius of our robot is 0.5 BL (approaching on-the-spot turning) thanks to the pectoral fins. This makes our robot more agile in yaw than several ones in both the miniature/low-cost and also the larger/more expensive categories, for example [1], [2], [3], [4], [7], [8].

Our descending (0.17 BL/s) and ascending (0.26 BL/s) rates are of the same order of magnitude as the forward swimming speed, eliminating potential bottlenecks in 3D trajectory following. A limitation of our depth variation mechanism is the need for dorsal fin actuation even when maintaining a 'fixed' depth, leading to reduced energy efficiency. One alternative mechanism for depth variation is pitching, which can be implemented by control surfaces [7] or by shifting the center of gravity [4]. However, using pitching couples depth variation with forward (or backward) motion, reducing maneuverability. Another mechanism for in-place depth variation is piston-based buoyancy modulation, which offers higher accuracy and energy efficiency than a dorsal fin, but at the price of added mechanical complexity (see Figure 8 in [6]). Given the results obtained, we consider our design choice as making a reasonable trade-off between depth variation accuracy, energy consumption, and robot complexity.

To sum up, we achieve considerably higher maneuverability than miniature robots [1], [2], [3], [4], and this allows to achieve complex autonomous control in 3D as we demonstrate in the next set of experiments.

B. Depth Control using a Pressure Sensor

Depth control is crucial for maneuvering in 3D, and elevates a robot's performance from simply swimming on the surface or diving uncontrollably. In our robot, depth control is achieved by using the dorsal fin in conjunction with feedback from a pressure sensor. We conducted two experiments, one to investigate long-duration depth maintenance (i.e., hovering), and the other to investigate long-range repeatable diving.

In the first experiment, the robot hovered at a set depth of 437 mm. The results shown in Figure 4 (left) indicate that depth maintenance is possible within half of a body height (30 mm). In the second experiment, the robot dove periodically between two thresholds set at 248 mm and 748 mm. The results shown in Figure 4 (right) demonstrate excellent accuracy and precision. The overshoots observed in this experiment can be explained by the robot's inertia, and the time delay introduced by smoothing the pressure sensor readings with an exponential moving average filter.

Summing the time when the dorsal fin was active results in approximately 20% on-time for hovering and 60% on-time for diving, although both conserve identical net potential energies. The discrepancy is mostly due to acceleration forces that build up while rising, and to a lesser extent due to increasing drag forces at higher rates of ascent/descent.

C. Navigation using an IMU

3D trajectory control is useful for moving an underwater robot from one place to another in space, for example while doing a systematic search over a small area. To demonstrate this we conducted a series of experiments including repeated square trajectories at a given fixed depth, and at incrementally decreasing depths. We also did additional experiments such as lawnmower-type (alternately turn 180° clockwise and counterclockwise) and a spiral-like (reduce side length after each completed square) search patterns, which are shown in the supplementary video.

All of these experiments relied on a basic architecture for control that includes a setup for sensor initializations,

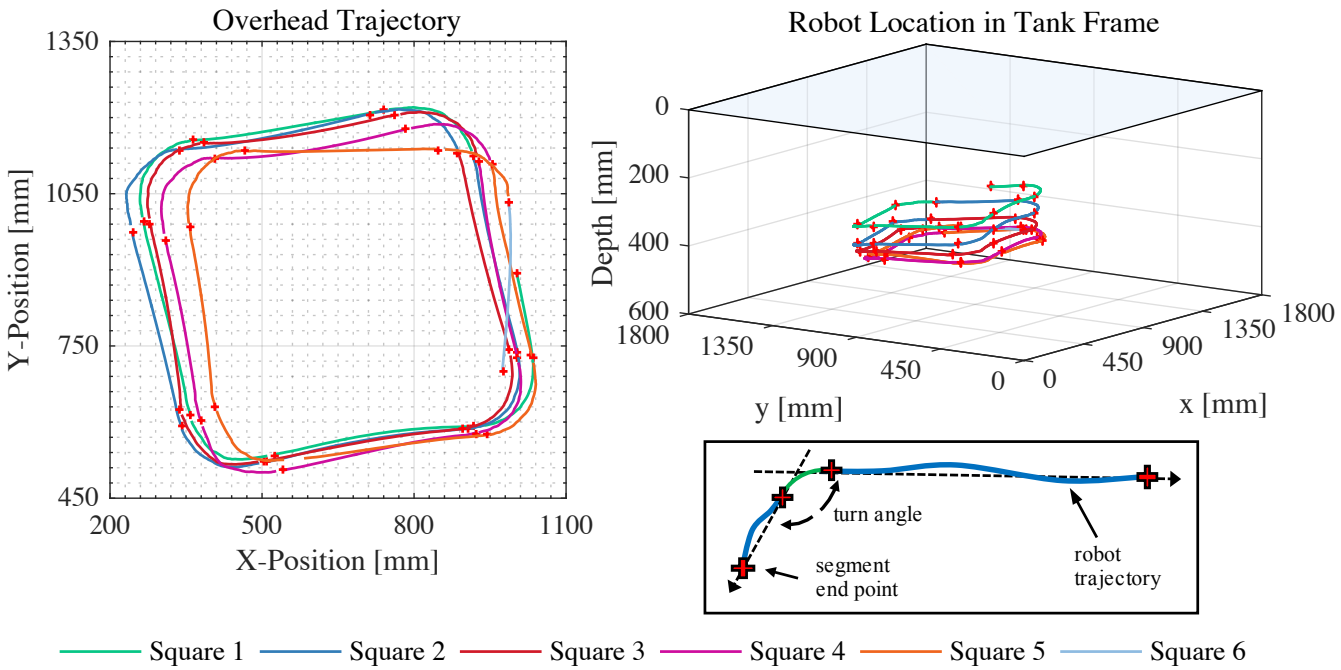

Fig. 5. **Left:** Robot trajectory for five complete squares in the x-y plane. **Upper Right:** 3D trajectory obtained via visual tracking from the overhead and side cameras. **Lower Right:** Robot trajectories were broken into straight segments (blue) and turn segments (green) based on the state of the controller. The turn angle is calculated using the vectors between segment end points (red crosses).

a main loop for high-frequency fin control, and a 10 Hz interrupt service routine, which defines robot behaviors based on sensor readings and logs data. The three basic behaviors are open-loop forward swimming, gyroscope-based turning, and pressure-based diving. A switch statement switches between forward, turning, and diving states whenever the respective thresholds corresponding to distance, angle, and depth are reached. The sensor readings were filtered with an exponential moving average filter (smoothing factor = 0.1).

To evaluate repeatability and drift over several repetitions of a prescribed trajectory, we used visual tracking in 3D and readings from the pressure sensor. This allowed us to know with high confidence where the robot was at all times in 3D space. The trajectories found using the visual tracking system were partitioned into straight swimming, turning, and rising segments based on the controller state, as shown in Figure 5 (lower right). The tracking videos were synchronized with the robot's on board data file using a sequence of LED flashes. By recording the LED and controller states throughout the experiment, the location in world coordinates where the robot changed state could be identified. Using the 3D coordinates and time stamps recorded along each segment of the trajectory, the segment lengths, swimming velocities, and turning angles could be calculated.

Complexities of moving in 3D space included coupled dynamics, such as the dorsal fin inducing undesired turning as a side effect of diving, imperfect straight forward motion, and drifting gyroscope readings. To mitigate the latter, an in situ drift model was obtained at the beginning of each experiment while the robot was at rest. The observed static drift in yaw was fitted with a linear regression to model its time-dependent progression, and then subtracted from the raw values. The final estimates used for turning during the experiments translated linearly to degrees, allowing us to set thresholds for any turning angle.

1) Swimming Repeated Squares at a Fixed Depth: Swimming repeated squares at a fixed depth resulted in high consistency between trajectories, as exhibited by Figure 5. During the experiment the robot executed five complete squares, with 20 turns of nominally 90°. All turns were between 96° and 82° with an average of 90° and a standard deviation of 4°. The average turning radius was 110 mm, or just over 1 BL. During the straight line segments of the squares, the robot swam without control for a period of 7.5 seconds at an average speed of 53 mm/s (0.53 BL/s). The robot speed was consistent across the 21 straight segments with a standard deviation of approximately 2 mm/s (0.02 BL/s), resulting in an average segment length of 388 mm (∼4 BL) with a standard deviation of 14 mm (∼0.1 BL). Because of the low deviation in turn angle and segment length, the squares were found to be largely repeatable with minimal rotation or drift in the prescribed shape.

2) Swimming Squares at a Incremental Depths: Figure 6 illustrates the trajectory of squares completed at incremental depths. The robot started at the bottom of the tank and decreased its depth by 200 mm after each completion of a square. Figure 6 (lower left) shows the depth of the robot found using pressure measurements and the target depth bands for each square. It was observed during the depth transitions that the heave and yaw motions of the robot were coupled. While the average turning angle was found to be 90°, equal to the fixed depth case, the standard deviation of the turning angle was 14° as opposed to 4° shown previously. This increased variation in turning angle was particularly prevalent in turning maneuvers

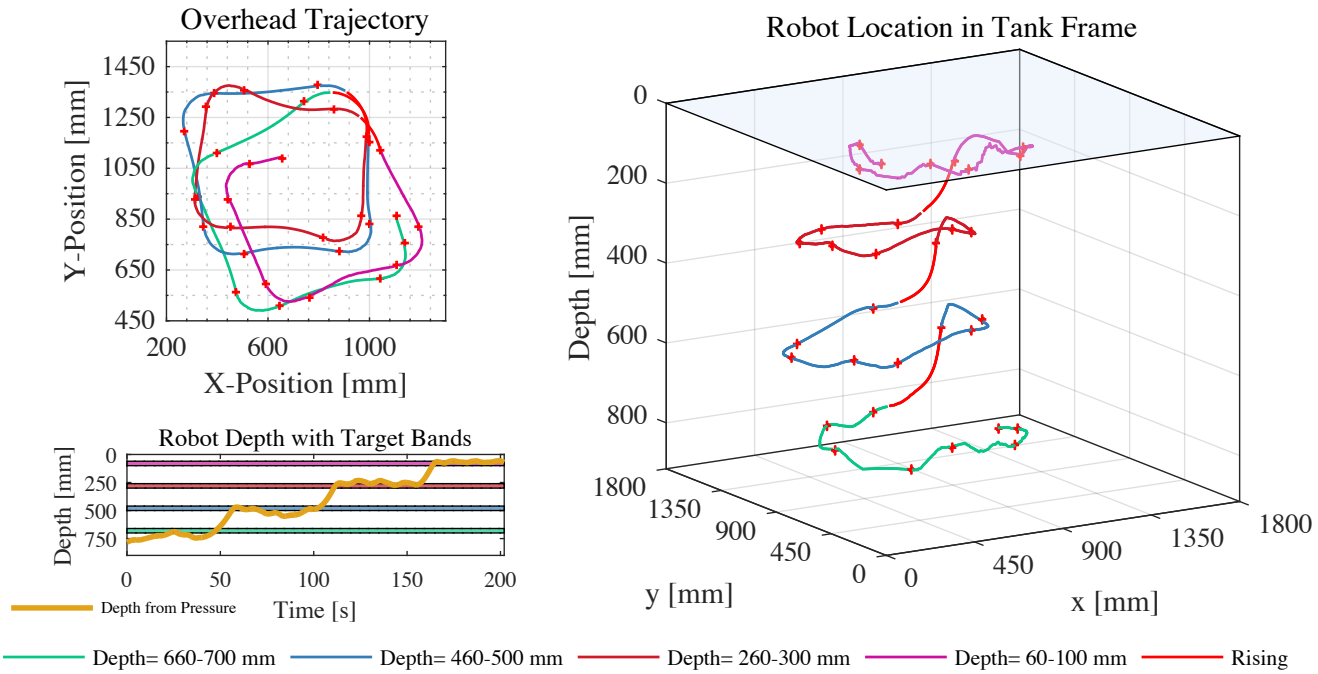

Fig. 6. **Upper Left:** Overhead view of robot trajectory during squares at incremental depths. **Lower Left:** Robot depth from the on-board pressure sensor (orange line) shown with target depth bands for each square. Depth band colors correspond to square colors above and at right. **Right:** 3D robot trajectory.

immediately following depth transitions (transitions shown in red in Figure 6, right), and introduced drift on the congruence of the squares. The average turning radius during the experiment was found to be 97 mm, or approximately 1 BL. While completing a square at each prescribed depth, the robot performed as expected, with an average swimming speed of 55 mm/s (0.55 BL/s) and an average segment length of 403 mm (∼4 BL), both consistent with previous experiments.

D. Homing to a Light Source using a Photodiode

Homing behaviors are a valuable primitive for enabling autonomous behaviors based on a global stimulus, such as autonomous charging or data transfer. To achieve homing, our robot has a front facing photodiode with a narrow viewing angle. The photodiode is used to perceive a light signal, which has the shape of a bell curve, peaking whenever the light is directly faced. The threshold for detection of the light source was either sampled during an initial 360° turn, or pre-set from a separate light characterization experiment. As a source, we used a 4-LED rod emitting blue light, which propagates best in water.

The robot control is programmed to turn left until the light intensity crosses the detection threshold, then swim towards the source. It starts turning again to realign with the source whenever the intensity value falls below the threshold for reasons such as drift. The implemented homing behavior allowed the robot to recover from any position, therefore guaranteeing robustness.

To test homing, we conducted the following experiment. We placed the LED rod at the south end and started the robot in the remaining three extremes of the tank (N,E,W), oriented in four directions (N,E,S,W). In total we did 48 trials. We measured success by seeing if the robot always reached an approximately two body length hemispherical zone surrounding the LED rod. Inside this zone, tracking was found to be unreliable as the blue light from the LED rod significantly altered the color of the robot in both the overhead and side videos.

Figure 7 shows a subset of 12 trajectories. We observed that the robot occasionally lost the LED rod, resulting in a full loop until it was reacquired. We consider the trials very successful because in each case, losing the LED rod was not fatal to the experiment's objective, and the robot successfully tracked to the hemispherical target zone, validating the robustness of the homing behavior.

The experiment was extended to moving back and forth between two sources, which were switched on and off alternately (see supplementary video). This extension hints towards the robot's potential to recover from a signal loss, realign with a source that changed position, or follow a moving source. Moreover, the robot's behavior may be interrupted and altered by a signal that is suddenly switched on, for instance to initiate homing.

E. Energy Efficiency

The robot uses a single battery (3.7 V, 320 mAh, 40x14x11 [mm]). We tested the battery lifetime for two experiments: (i) swimming submerged using several fins at the same time lasted 25 min; (ii) submerged hovering only using the dorsal fin ran for 69 min. These were the experiments illustrated in Figures 4 and 5 respectively. Hence, active depth control costs 25/69 = 36% ≈ 1/3 of battery runtime, which may be expected considering that the dorsal fin uses one MIC actuator and the caudal fin uses two.

There are several ways to increase runtime. Currently we are adding 25 g to the robot to achieve neutral buoyancy; those might be replaced by additional batteries in the future.

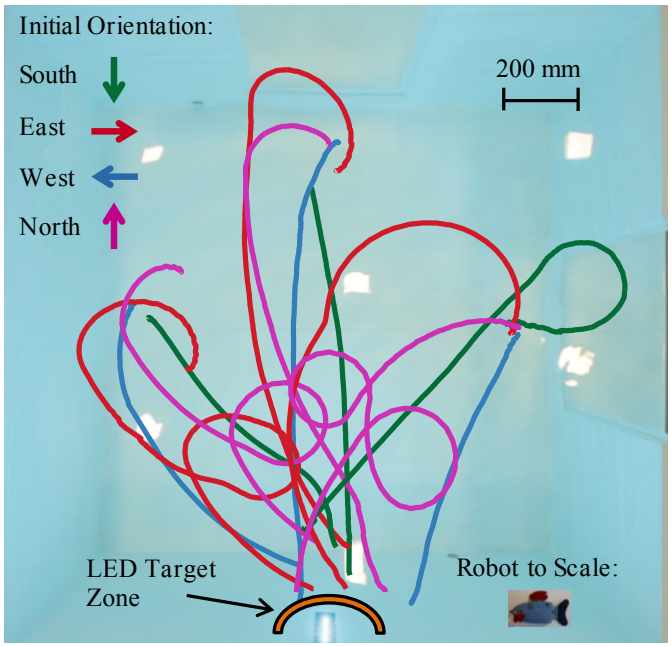

Fig. 7. Ensemble of the trajectories from twelve LED homing experiments. Experiments were conducted using four initial orientations (denoted by trajectory color), and from initial positions near the center of each of the three unlit tank walls. Experiments were ended when the robot reached a hemispherical zone surrounding the LED rod denoted in orange.

Another potential energy savings can come from more efficient control signals; operating the MIC propulsors with pulse-width-modulation instead of bang-bang control shows the potential to extend the runtime towards 2 h saving 45% in energy [2].

VI. Conclusions and Future Work

We developed a miniature robot using a set of four MIC propulsors to achieve high 3D maneuverability underwater. The MIC propulsors allowed for a reduction in mechanical complexity compared to traditional rotary shaft actuators by eliminating the need for a shaft exit through the watertight hull, and are low-cost at $1 per propulsor. The swimming performance of the robot was validated through a series of trials following prescribed 3D paths at consistent and variable depths. Using a visual tracking system and data from on-board sensors, the robot was found to have a forward swimming speed of 0.6 BL/s and a minimum turning radius of 0.5 BL. Using pressure sensor feedback, the actuated dorsal fin for diving (0.17 BL/s), and the positive buoyancy for ascent (0.26 BL/s), the depth of the robot could be controlled within target bands of approximately 1/2 of a body height (30 mm). Successful homing towards an LED rod was demonstrated from a range of starting positions and orientations using feedback from a photodiode mounted on the robot's front, demonstrating the potential for neighbor following, beacon tracking, and local fencing based on optical cues. Our robot achieves smaller size and lower cost than [6], [7], [8], [9], while also achieving higher maneuverability than miniature robots like [1], [2], [3], [4].

Design and hardware integration choices for the underwater robot were driven by utilization of the design as the agent robot in a laboratory swarm testbed. This study validates that the current configuration of multiple MIC propulsors can provide the robust maneuverability necessary for the formation and maintenance of future 3D collectives. Increased integration of the MIC propulsors with body and fin design could enhance the overall vehicle hydrodynamics, leading to increased speed.

Exploring the minimal sensing and communication hardware necessary to enable self-organizing behaviors is the next step in the realization of an underwater collective testbed, and represents an ongoing area of research. In addition to hardware advances, algorithms for self-organizing behaviors by non-holonomic agents in a sensory-deprived environment are being developed. Applying the algorithmic knowledge gained from the laboratory testbed will reduce the difficulties associated with real-world deployment of sophisticated collectives in high-risk marine environments.

References

[1] V. Kopman and M. Porfiri, "Design, Modeling, and Characterization of a Miniature Robotic Fish for Research and Education in Biomimetics and Bioinspiration," *IEEE/ASME Transactions on Mechatronics*, vol. 18, no. 2, pp. 471–483, Nov. 2012.

[2] A. J. Clark, X. Tan, and P. K. Mckinley, "Evolutionary multiobjective design of a flexible caudal fin for robotic fish," *Bioinspiration and Biomimetics*, vol. 10, no. 6, pp. 1–17, Nov. 2015.

[3] M. Aureli, V. Kopman, and M. Porfiri, "Free-Locomotion of Underwater Vehicles Actuated by Ionic Polymer Metal Composites," *IEEE/ASME Transactions on Mechatronics*, vol. 15, no. 4, pp. 603–614, Sep. 2009.

[4] Y. Takada, K. Koyama, and T. Usami, "Position Estimation of Small Robotic Fish Based on Camera Information and Gyro Sensors," *Robotics*, vol. 3, no. 2, pp. 149–162, Jun. 2014.

[5] S. A. Watson and P. N. Green, "Propulsion systems for micro-Autonomous Underwater Vehicles (μAUVs)," in *2010 IEEE Conference on Robotics, Automation and Mechatronics (RAM)*, 2010, pp. 435–440.

[6] S. Mintchev, E. Donati, S. Marrazza, and C. Stefanini, "Mechatronic design of a miniature underwater robot for swarm operations," *2014 IEEE International Conference on Robotics and Automation (ICRA)*, pp. 2938–2943, 2014.

[7] "The Jessiko project," http://www.robotswim.com/index.php, accessed: 2017-02-07.

[8] Y. Hu, W. Zhao, G. Xie, and L. Wang, "Development and target following of vision-based autonomous robotic fish," *Robotica*, vol. 27, no. 07, pp. 1075–1089, 2009.

[9] S. Bhattacharyya and H. Asada, "Control of a compact, tetherless ROV for in-contact inspection of complex underwater structures," *2014 IEEE/RSJ International Conference on Intelligent Robots and Systems (IROS)*, pp. 2265–2272, 2014.

[10] T. Treibitz, Y. Y. Schechner, and H. Singh, "Flat refractive geometry," in *2012 IEEE Conference on Computer Vision and Pattern Recognition (CVPR)*. IEEE, 2008, pp. 1–8.

[11] R. J. Clapham and H. Hu, "isplash-ii: Realizing fast carangiform swimming to outperform a real fish," in *2014 IEEE/RSJ International Conference on Intelligent Robots and Systems (IROS)*, Sept 2014, pp. 1080–1086.